Tuning the Radiative Lifetime in InP Colloidal Quantum Dots by Controlling the Surface Stoichiometry

Panagiotis Rodosthenous,[†] Francisco M. Gómez-Campos,[‡,¶] and Marco Califano[*,†,§]

† *Pollard Institute, School of Electronic and Electrical Engineering, University of Leeds, Leeds LS2 9JT, United Kingdom*

‡ *Departamento de Electrónica y Tecnología de Computadores, Facultad de Ciencias, Universidad de Granada, 18071 Granada, Spain*

¶ *CITIC-UGR, C/ Periodista Rafael Gómez Montero, n 2, Granada, Spain*

§ *Bragg Centre for Materials Research University of Leeds, Leeds LS2 9JT, United Kingdom*

E-mail: m.califano@leeds.ac.uk

Abstract

InP nanocrystals exhibit low photoluminescence quantum yield. Like in the case of CdS, this is commonly attributed to their poor surface quality and difficult passivation, which give rise to trap states and negatively affect emission. Hence the strategies adopted to improve their quantum yield have focussed on the growth of shells, to improve passivation and get rid of the surface states. Here we employ state-of-the-art atomistic semiempirical pseudopotential modelling to isolate the effect of surface stoichiometry from features due to the presence of surface trap states, and show that, even with an atomistically perfect surface and an ideal passivation, InP nanostructures may still exhibit very long radiative lifetimes, of the order of tens of microseconds, broad, weak emission and large Stokes' shifts. Furthermore, we find that all these quantities can be varied by orders of magnitude, by simply manipulating the surface composition, and, in particular, the number of surface P atoms. As a consequence it should be possible to substantially increase the quantum yield in these nanostructures by controlling their surface stoichiometry.

Graphical TOC Entry

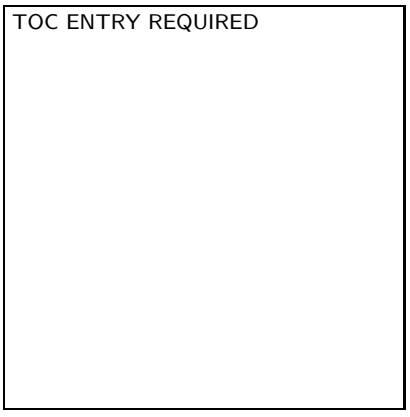

Semiconductor Colloidal Quantum Dots (CQDs) have drawn great attention due to their unique size-dependent electronic and optical properties which make these nanocrystals (NCs) ideally suited for a wide range of applications[1,2] such as lighting, photovoltaics, catalysis, optoelectronics and bio-imaging. In particular InP has emerged as a promising environmentally-friendly material[3,4] that could replace cadmium-based semiconductors, such as CdSe, CdTe and CdS, whose toxicity will limit the commercialisation in many countries.[5] InP is a direct bandgap semiconductor with a larger dielectric constant, lower effective electron and hole mass, weaker phonon coupling and lower toxicity than chalcogenide-based semiconductors. It has a similar bandgap to CdSe, with which also shares a size-tunable emission in the visible region of the spectrum.[4]

Although the electronic and optical properties of nanoscale InP were first investigated experimentally by Micic *et al.*,[6] and theoretically by Fu and Zunger,[7] over 20 years ago, the interest in this material is still high, with applications of InP NCs ranging from optoelectronics[8] to photovoltaics,[9] and from bio-imaging[10] to memory storage[11] and lighting.[12] Nevertheless, the measured photoluminescence (PL) quantum yield (QY) is still low especially in small (< 3 nm) QDs,[12–16] and the presence of deep-trap emission is still reported even in core/shell systems.[17–20] Only very recently Jang's group[20,21] and Peng's group[8] were able to achieve nearly 100% PL QY in InP/ZnSe/ZnS QDLEDs. The record QY was attributed to an improved surface passivation achieved by means of the multilayer shell structure, where the ZnSe interlayer served as strain reliever between InP and ZnS, resulting in the elimination of most surface defects. In general, however, InP-based QLEDs exhibit low efficiency, due to the low QY which results from decreased radiative recombination rates. These are generally ascribed to the presence of surface traps, due to imperfect passivation.[3,10,22,23] It is however still unclear what kind of traps (electron or hole) are present on the surface[22,24,25] and what are the origins of the broad, red-shifted emission (Stokes' shift) observed in many samples.

In this work we present a detailed theoretical characterisation of InP CQDs, focussing

in particular on the effects of surface stoichiometry on the optical properties and excited state relaxation. We show that, even in the presence of a full coverage of ideal passivants, i.e., in the absence of surface traps, the radiative recombination times in InP NCs can be as long as tens of microseconds, and depend on the surface composition, i.e., on whether there is a prevalence of In or P atoms on the surface. Strikingly, we find that the addition of only a few P atoms on an otherwise In-rich surface can reduce (i) the radiative lifetime (by about two orders of magnitude), (ii) the Stokes' shift and (iii) the PL linewidth, in small NCs, where the surface atoms represent a substantial fraction of the total number of atoms. In larger structures, the effect of surface stoichiometry becomes less important and is balanced by the increase of the volume.

Our NCs are built atomistically, according to the InP bulk crystal structure, from a central anion up to the desired radius. This method of generating the atomic positions yields unsaturated bonds at the surface, which are passivated using pseudo-hydrogenic, short-range potentials with Gaussian form (further details are provided in the Supporting Information). In this work we developed new passivation parameters (see Table S1 - Supporting Information), with improved confinement compared with those available in the literature.[7,26] The single-particle energies and wave functions are obtained by solving the Schrödinger equation using the state-of-the art plane-wave semiempirical pseudopotential method,[27] including spin-orbit coupling. The optical spectra and radiative lifetimes are calculated via a configuration interaction scheme, including excitonic effects.[28]

The thermally averaged lifetimes are calculated assuming Boltzmann occupation of higher-energy excitonic states, separated by an energy ΔE_γ, as

$$\frac{1}{\tau_R(T)} = \frac{\Sigma_\gamma (1/\tau_\gamma) e^{-\Delta E_\gamma / k_B T}}{\Sigma_\gamma e^{-\Delta E_\gamma / k_B T}} \tag{1}$$

where the radiative lifetime τ_γ for the transition from the excitonic state Ψ_γ to the ground state is obtained in the framework of time-dependent perturbation theory as

$$\frac{1}{\tau_\gamma} = \frac{4nF^2\alpha\omega_\gamma^3}{3c^2\left|M_\gamma\right|^2}, \tag{2}$$

α is the fine structure constant, $\hbar\omega_\gamma$ is the transition energy, c is the speed of light in vacuum, $\mid M_\gamma \mid$ is the dipole matrix element of the excitonic transition, n is the refractive index of the surrounding medium, $F = 3\epsilon/(\epsilon_{dot} + 2\epsilon)$ is the screening factor, $(\epsilon = n^2)$, and ϵ_{dot} is the dielectric constant of the nanocrystal which is calculated using a modified Penn model.[28]

Auger decay times are calculated within the standard time-dependent perturbation theory according to the formalism developed in ref. [29]

$$(\tau_{\mathrm{A}})_i^{-1} = \frac{\Gamma}{\hbar}\sum_n \frac{|\langle i|\Delta H|f_n\rangle|^2}{(E_{f_n} - E_i)^2 + (\Gamma/2)^2}. \tag{3}$$

where $|i\rangle$ and $|f_n\rangle$ are the initial and final states, E_i and E_{f_n} are their energies, ΔH is the screened Coulomb interaction and $\hbar/\Gamma$ is the lifetime of the final states ($\Gamma = 10$ meV was used here[30]). In the regional screening used in the calculation of the Auger integrals[29] a value of 2.5 (representative of most capping groups and solvents) was assumed for the dielectric constant outside the dot.

We consider spherical NCs with radii ranging from 10 Å to 30 Å. The calculated position of their band edges as a function of size is presented in Fig. 1, from which it is clear that our nanostructures are free from (trap) states in the gap.

This is also confirmed by the three-dimensional visualization of the charge density (central panels in Fig. 1), clearly exhibiting no localisation on the surface, hence indicating the absence of surface states. The charge density distribution of both CBM and VBM within the different nanostructures, was determined by integrating the square of the re-

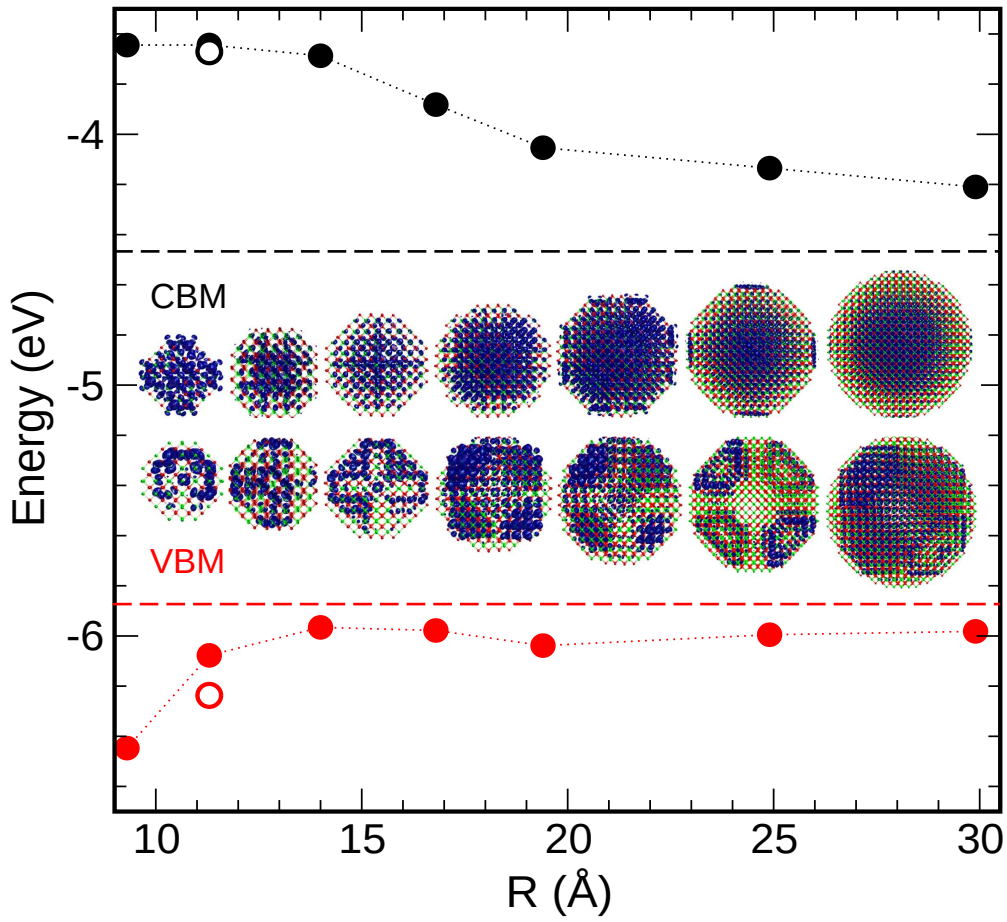

Figure 1: Calculated band edge energies as a function of NC size (The corresponding 3D charge densities are presented in blue in the central panel, where green dots represent P atoms and red dots In atoms). The dashed lines represent the position of CBM (black) and VBM (red) in bulk InP. The empty circles mark the band edges' position in a NC with $R = 12$ Å, after adding 6 P atoms on the NC surface (see text).

spective wave functions within spheres (concentric with the NC) with increasing radii up to the NC radius R. We found much lower values for the charge density of the VBM compared to the CBM within 80% of R for all sizes except the smallest NC (see Table 1).

Table 1: CBM and VBM charge densities (%) calculated, in all the CQDs investigated, as integrals of the square of the respective wave functions within spheres (concentric with the NC) with radii R_{int} ranging from 50% to 90% of the NC radius R. The surface character (whether cation- or anion-rich) is also shown for each NC. As an example, in an InP NC with radius 14 Å (with an In-rich surface) 42% of the CBM and only 7.9% of the VBM are localised within a sphere with a radius of 8.4 Å (i.e., 60% R). We therefore conclude that most of the VBM charge density in this dot is contained outside it, i.e., in a spherical shell with inner radius = 8.4 Å and outer radius $= R$.

	$R = 9.3$ Å P-rich		$R = 14$ Å In-rich		$R = 16.8$ Å In-rich		$R = 19.4$ Å P-rich		$R = 24.9$ Å In-rich		$R = 29.9$ Å P-rich	
R_{int}	CBM	VBM	CBM	VBM	CBM	VBM	CBM	VBM	CBM	VBM	CBM	VBM
90	60.3	87.8	86.1	87.1	84.9	77.4	76.8	71.1	87.7	70.8	90.2	86.7
80	39.6	58.1	71.8	51.8	67.5	36.9	60.8	41.6	74.7	25.4	77.9	67.8
70	21.6	32.5	56.0	19.3	53.1	19.8	47.1	23.8	58.7	7.7	62.6	48.2
60	11.9	17.9	42.0	7.9	39.1	8.2	33.8	21.0	42.5	1.9	46.2	30.5
50	6.6	7.7	28.6	2.5	25.9	3.4	21.6	6.2	27.5	0.4	30.7	16.2

Indeed, despite the ideal passivation we used to confine both electron and hole to the core region of the dot, we find that the presence of P atoms creates a strong repulsive potential for the hole, pushing its charge density towards the surface, in the case of prevalently In-terminated NCs. For P-rich surfaces, instead, the opposite occurs, and the hole localises more in the dot core. The electron charge density, for which P act as an attractive potential, is instead always mostly confined to the core, but exhibits some additional surface localisation in the presence of P-rich surfaces. These effects can be clearly observed qualitatively in the charge density distributions presented in Fig. 1 (where green dots represent P atoms and red dots In atoms). A more quantitative comparison is presented in Table 1, where the larger difference exhibited between the spatial distribution of the charge densities of VBM and CBM in NCs with In-rich surfaces, compared with P-terminated dots, is especially evident in the inner core (for $R_{\text{int}} \leq 70\%$R), i.e, within

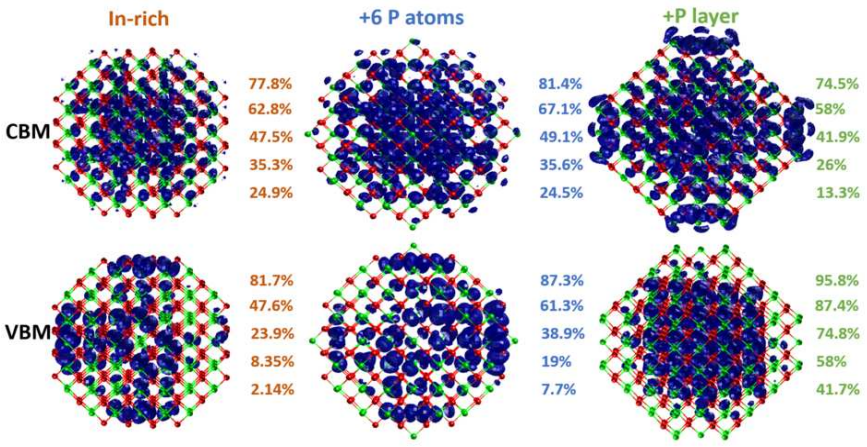

Figure 2: Evolution of the calculated CBM and VBM charge densities (blue) in an InP CQD with $R = 11.3$ Åwith increasing P surface coverage, from an In-rich surface to a full P layer coverage (green dots represent P atoms and red dots In atoms): the numbers next to each charge density plot quantify the charge density (as a percentage of the total charge density) calculated within spheres, concentric with the NC, with radii equal to 90%, 80%, 70%, 60% and 50% of the dot radius R, similarly to the results presented in table 1.

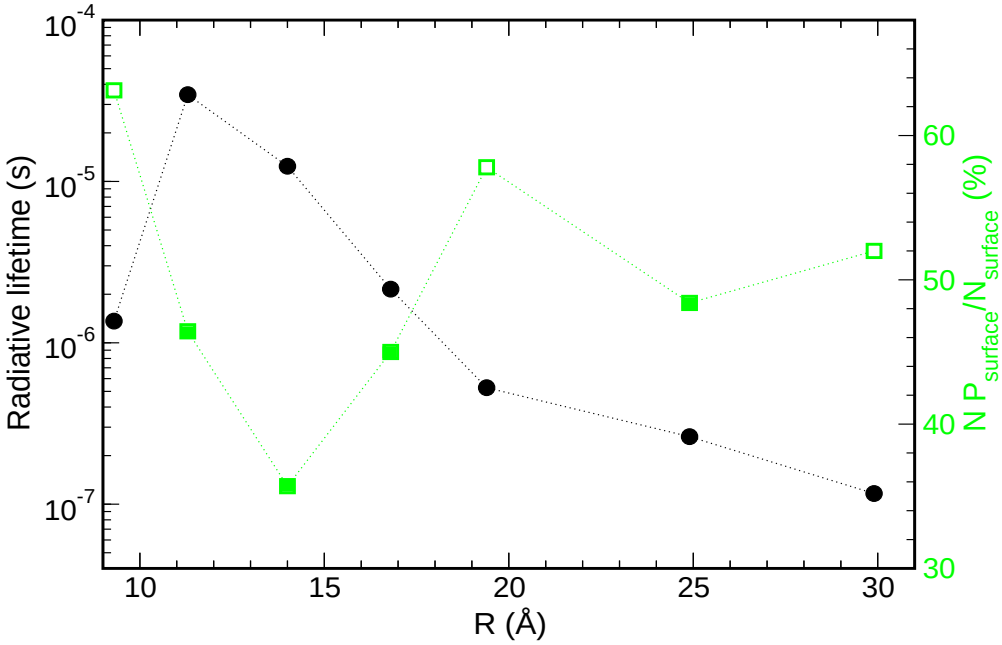

Figure 3: Room temperature radiative lifetimes (black circles, left y axis) calculated as a function of QD radius. The fraction of P surface atoms as a percentage of the total surface atoms (green squares, right y axis) is also displayed. Full squares represent P fractions below 50% (i.e., In-rich surfaces), whereas empty squares indicate P fractions above 50% (i.e., P-rich surfaces).

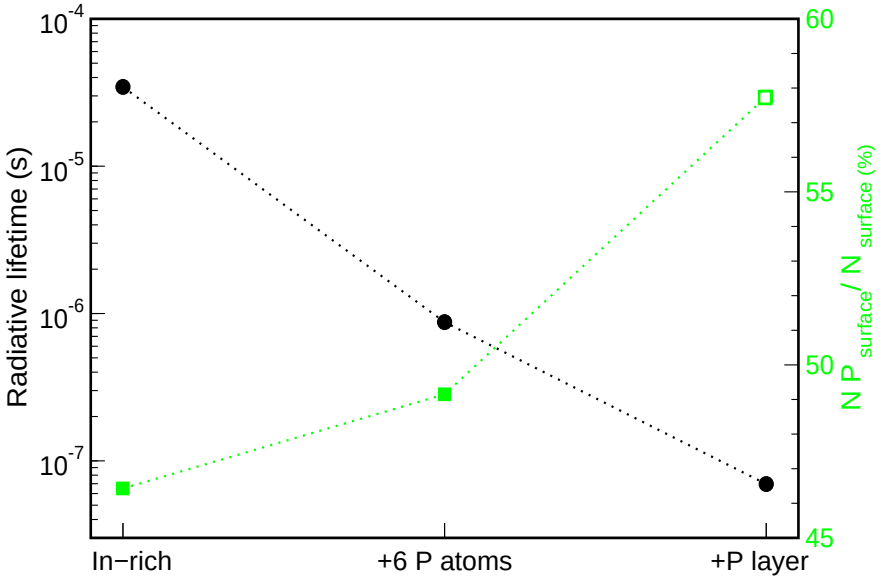

Figure 4: Evolution of the calculated radiative lifetime of an InP CQD with $R = 11.3$ Åwith increasing P surface coverage, from an In-rich surface to a full P layer coverage. The calculated charge densities of both CBM and VBM relative to the 3 different cases considered are displayed in Fig. 2.

spherical volumes with radii $\leq$ 70%R. This difference is also confirmed by the shifts predicted in the band edges positions (see empty circles in Fig. 1) following the addition of a single P atom on every equivalent (100) In-terminated facet, for a total of 6 surface P atoms:[31] while the VBM moves away from the bulk VBM to more negative energies, indicating an increase in confinement, the CBM moves closer to the bulk CBM, as a consequence of decreased confinement. The effect of the surface stoichiometry on the band edges' wave functions is summarised in Fig. 2, which shows the charge density evolution with increasing surface P coverage from In-rich surfaces to P-rich surfaces: in the former case (left panel) the CBM is well confined to the dot core and the VBM exhibit regions of large charge density close to the surface, whereas in the P-rich case (right panel) the opposite is true.

The origin of this effect is the peculiar nature of P, when compared to other widely used group V anions (e.g., As, Sb, etc.). Its electronic configuration is $1s^2 2s^2 2p^6 3s^2 3p^3$: i.e., like all the other anions (see Table S2, Supporting Information), it has a p-like outer

shell, however, unlike other anions, P (like S) has no d-like orbitals. From this point of view comparing In-based pnictogen NCs and Cd-based chalcogen NCs, InP CQDs are more similar to CdS NCs[32] than to CdSe dots. Therefore, it is perhaps not a coincidence that both InP and CdS are plagued by trap states,[17–19,22,24,25,33–35] which have proven difficult to eliminate experimentally despite the best efforts at passivating their surface. In addition In and P have large differences in the electronic properties (the outermost electronic configuration of In is $4d^{10}5s^25p^1$, which also contains d-like orbitals) atomic size, and in the electron affinity and ionization potential. In this light, recent density functional theory (DFT) calculations[36] predicted a difference in crystal potential between In- and P-terminated InP dots in the presence of oxidised surfaces.

As a consequence of the relative displacement between the charge densities of VBM and CBM, where the former is more localised on the core outer shell and the latter more in the core centre (as shown in Fig. 1), the overlap between their wave functions is strongly reduced, leading in extreme cases (i.e., for small NC sizes with In-terminated surfaces) to (i) a completely dark[37] ground state exciton manifold (i.e., the 8 exciton states derived from $(e_1, h_{1,2})$ - where e_1 is the CBM and $h_{1,2}$ is the doubly degenerate VBM - are all optically forbidden), and (ii) tens-of-microseconds-long radiative lifetimes (Fig. 3). We note that these features are not an artefact of our specific choice of passivants, as they also emerge using the passivation set from Graf *et al.*[26] Interestingly we find that both these effects are correlated to the fraction of P surface atoms, at least for small NC sizes, where to larger fractions correspond brighter excitons and faster radiative recombinations. The confining effect of surface P on the VBM wave function is so strong that, in the case of $R = 12$ Å where the surface is In-rich, the simple addition of a single P atom on every equivalent (100) In-terminated facet[31] (for a total of 6 added P atoms) leads to a reduction in the radiative recombination time by over one order of magnitude, from tens of microseconds to hundreds of nanoseconds. A further increase of P surface coverage leads to an even faster recombination, of the order of tens of nanoseconds (Fig. 4) and to a

full recovery of a bright exciton in the ground state manifold. This effect is stronger for smaller sizes, where the surface atoms represent a substantial fraction of the total number of atoms. In larger structures the effect of surface stoichiometry becomes less important and the radiative lifetime is the result of a combination of surface effects and volume increase (a comparison between radiative lifetimes calculated in NCs with P-rich and In-rich surfaces is presented in Fig. S1, Supporting Information). Indeed we find that, as it is the case for other materials (such as CdSe[38] and GaSb[39]), τ_{rad} decreases with increasing dot size.

These findings seem to find support from (and, at the same time, may be able to provide additional insight into) recent measurements of lower PL QYs in In-rich (compared with stoichiometry-controlled) InP/ZnSe core/shell and InP/ZnSe/ZnS core/shell/shell NCs.[8] The difference between the QYs in the two systems was shown to be due to the gradual In incorporation in the epitaxially grown ZnSe and ZnS shells that occurred in NCs synthesised using the conventional route, but not in those obtained using a stoichiometry-controlled synthesis. The presence of In atoms (known electronic dopants for II-VI materials) in the shell(s) was assumed to generate intra-gap states, leading to non-radiative recombination, hence to QY degradation. Our results discussed above suggest the presence of a possible additional component to the QY reduction in In-rich samples, especially considering the small size of the InP core ($R = 1.4$ nm) in those experiments.

The NC surface stoichiometry does not affect appreciably, instead, the position of the absorption edge (as shown in Fig. 5A, where the red circles indicate our results - the empty red circle represents the calculated band gap after the addition of 6 P atoms on the surface), as the bright transitions it corresponds to have similar energies for all surface terminations. These transitions, however, are not to the same states. Indeed, for smaller, In-terminated dots, the first optically allowed transition occurs to an exciton state (different for the different sizes) that is contributed to by either highly excited hole states and the CBM ($|h_j; e_{\text{cbm}}\rangle$), or by the VBM and excited electron states ($|h_{\text{vbm}}; e_k\rangle$), precisely

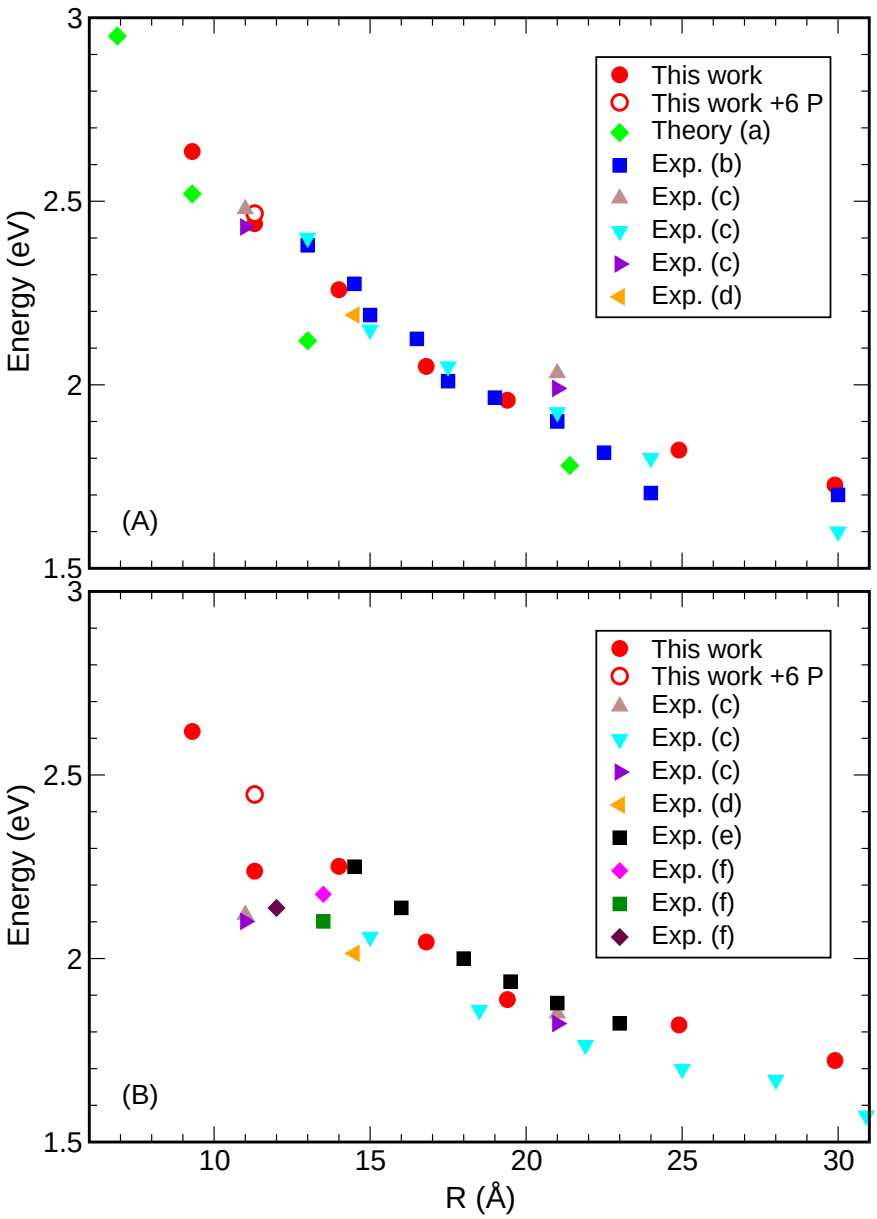

Figure 5: Absorption (A) and emission (B) spectra: comparison of our results (red circles) with experimental (coloured symbols) and theoretical (green diamonds) studies. (a): [7]; (b): [6]; (c): [40]; (d): [17]; (e): [41]; (f): [42].

owing to the aforementioned relative displacement between the charge densities of VBM and CBM, which yields a small overlap between them. This leads to large Stokes' shifts and weak PL intensities for these nanostructures, as the emission always originates from the dark[37] ground state manifold which is located at a much lower energy (see Fig. 6a, where we show both absorption - blue lines - and emission - red lines - spectra calculated for a $R = 11.3$ Å NC with an In-rich surface). In NCs with P-rich surfaces, instead, an optically allowed exciton state exists within the ground state manifold, leading to small Stokes' shifts, and stronger and faster emission (see Fig. 6b - same NC as in Fig. 6a, but with inverted stoichiometry).

In one of the seminal papers by Nozik's group,[43] InP NCs were prepared using both excess In and excess P in their synthesis, however, in that study it had been impossible to separate the effects of surface stoichiometry from those of the presence of trap states, on the optical properties. Indeed, as the capping agent used (TOPO) coordinates mainly with In^{3+} surface ions, the presence of excess P was associated by Micic *et al.*[43] with incomplete surface passivation, which leads, *inter alia*, to a broad size distribution, hence to a broad PL spectrum. On the other hand, in NCs prepared with excess In^{3+}, the presence of an additional broad PL feature at low energies was attributed to radiative surface states produced by phosphorus vacancies.[25,43] Nevertheless, they were still able to conclude that the Stokes' shifts they observed between the emission peak and the first absorption peak were related to core effects, and did not depend on the presence of any surface trap, as their magnitude did not change after treatment with HF or other etchants.

In general, due to the presence in experimental samples of a mixture of In- and P-terminated NCs, and of a distribution of sizes, the emission is often broad and the observed Stokes' shift consequently small. In Fig. 6 we show how, for the case of an InP NC with $R = 11.3$ Å, the relative positions of optical transitions and corresponding spectral peaks depend crucially on the value of the experimental linewidth: large linewidths mask the actual position of the optical transitions, resulting in a blue-shift of the PL peak and

in a consequent reduction of the observed Stokes' shift. Smaller linewidths, still within experimental capabilities,[43,44] allow to recover the *real* position of the optical transitions providing a more accurate PL energy. This could explain why the position of the PL measured by different groups (or in different samples by the same group) in dots with the same nominal size exhibits a wide range of variation, as shown in Fig. 5B, compared with that of the absorption edge (Fig. 5A).

In general, Auger processes (Auger Recombination, AR, and Auger electron Cooling, AC) are very efficient in CQDs: in CdSe NCs, observed AR times range from a few to a few hundreds of picoseconds (they are even faster in NCs made of other semiconductor materials[46,47]), whereas AC times are of the order of hundreds of femtoseconds,[29,48] and they all increase with NC size.

In contrast with these expectations, and consistently with our findings relative to the radiative lifetimes, we find longer Auger lifetimes than usual for both processes: our calculated Auger recombination times range from about 120 ps for $R = 9.3$ Å, to 2080 ps for $R = 24.9$ Å, and although they follow the observed trend with NC size highlighted by Klimov's group,[49] they are about at least one order of magnitude slower, if compared with what is observed in CdSe NCs,[48] and two to three orders of magnitude larger than the AR lifetimes in InSb.[46,47] This is shown in Fig. 7, where, following Robel *et al.*,[49] we plot the Auger constant C_{A}, defined as

$$C_{\mathrm{A}} = \frac{V_0^2}{(8\tau_{AR})} \tag{4}$$

(where V_0 is the NC volume and τ_{AR} is the AR lifetime), as a function of dot size.

Unfortunately, this strong suppression of AR is accompanied, as discussed above, by a similar suppression of radiative recombination, resulting in an overall faster AR channel.

Similarly, our predicted AC lifetimes are about one order of magnitude longer than in

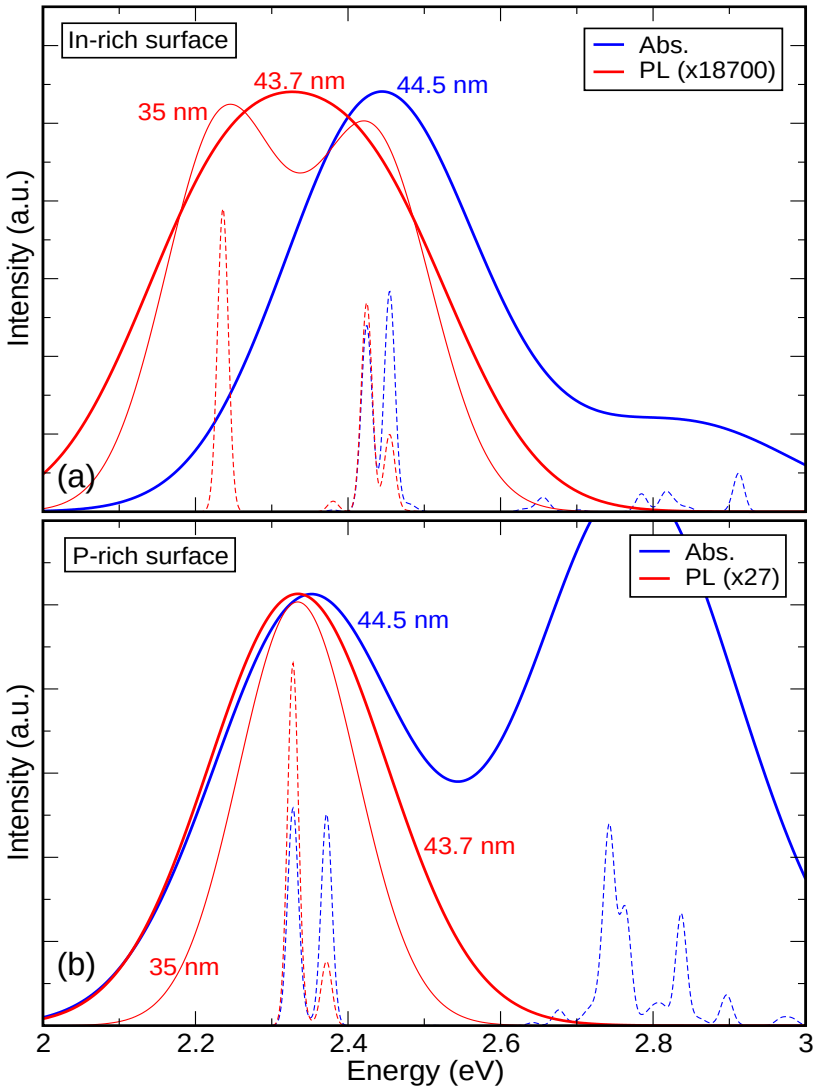

Figure 6: Room temperature absorption (blue lines) and emission (red lines) spectra for an InP NC with $R = 11.3$ Å with an In-rich (top panel) and a P-rich (bottom panel) surface. The top structure is anion-centred, the bottom one has an inverted stoichiometry (i.e., anions and cations are interchanged) and is cation-centred. The spectra are calculated for different experimental linewidths (44.5 nm,[45] thick blue lines; 43.7 nm,[45] thick red lines; and 35 nm,[44] thin red lines), and also using a much smaller - and, so far, experimentally unachievable - linewidth (17 meV, dashed lines), in order to show how the relative positions of optical transitions and spectral peaks may vary, depending on the value of the linewidth. The PL amplitude has been normalised to that of the first absorption peak by multiplying it by a factor of 1.87×10^4 (top panel) or 27 (bottom panel), i.e., the PL amplitude in the NC with an In-rich surface is about 3 orders of magnitude smaller than that in the NC with a P-rich surface.

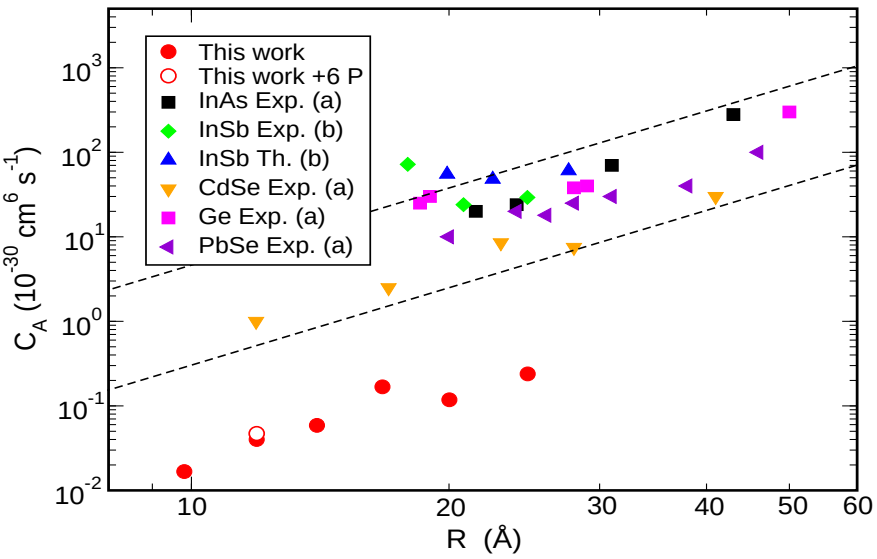

Figure 7: Auger Constant as a function of QD radius: comparison with experiment. (a): [49]; (b): [46]. The dashed lines indicate the universal scaling boundaries from Robel *et al.*[49]

CdSe,[29,48] ranging from a few hundreds of femtoseconds to a few picoseconds (see Fig. S2, Supporting Information). The only exception is represented by $R = 14$ Å, in which the first electron excited state has an *s*-like character and is singly degenerate, in contrast to the (nearly) 3-fold degenerate *p*-like states that are found in all other sizes, resulting in a much longer lifetime than in all other dots considered in this study. We find that the details of the surface stoichiometry have a weaker effect on all Auger processes than they have on the emission properties (compare empty and solid red circles in Fig. 7 and Fig. S2, Supporting Information), as the former involve both band edge and excited states, whose charge densities normally exhibit a relative displacement.

In conclusion, we have shown that small InP NCs with an ideally passivated P-rich surface exhibit faster radiative recombination, stronger emission and smaller Stokes' shifts compared to NCs whose surface has a prevalence of In atoms. The latter show long lifetimes and weak emission despite the presence of a full passivant coverage, i.e., in the absence of any trap states, owing to the existence of a relative displacement between the charge densities of CBM and VBM (hence a reduced coupling between them), that gives

rise to a completely dark ground state exciton manifold extending over a considerable energy window. Our results therefore suggest that, in such NCs, commonly adopted strategies to improve emission QY by removing surface traps may fail if they do not, at the same time, provide additional confinement for the hole. Indeed, recent InP/ZnSe/ZnS core/multiple-shell structures exhibiting near-unity QYs, successfully address both issues: they minimise the number of defects by preventing oxidation and strain formation at the heterojunctions, on the one hand, and, on the other hand, by exploiting the large valence band offset (of the order of 1 eV[50]), between core and shell material, they provide strong additional confinement for the hole. HF treatment on its own, however, only addresses the first issue, as it removes undercoordinated surface P atoms, responsible for the formation of gap states. Although this may lead to a relative improvement in the PL efficiency,[51] HF etching results in In-rich surfaces,[51] and we have shown here that, even in ideally passivated NCs, such a surface stoichiometry, adversely affects hole confinement, thereby compromising the emission.

We propose that this effect is particularly strong in InP NCs due to the peculiar electronic structure of P atoms which, like that of S, lacks *d* orbitals.

Supporting Information Available

Passivation procedure and parameters, Electronic configuration of the outer shell of the anions most commonly found in semiconductor NCs, Radiative lifetimes for different surface stoichiometries, Calculated Auger Cooling times.

Acknowledgements

P.R. gratefully acknowledges financial support from EPSRC through a Doctoral Training Grant.

References

(1) Talapin, D.V.; Lee, J.; Kovalenko, M. V.; Shevchenko, E. V. Prospects of Colloidal Nanocrystals for Electronic and Optoelectronic Applications. *Chem. Rev.* **2010**, *110*, 389-458.

(2) Kovalenko, M. V.; Manna, L.; Cabot, A.; Hens, Z.; Talapin, D.V.; Kagan, C. R.; Klimov, V. I.; Rogach, A. L.; Reiss, P.; Milliron, D. J.; et al. Prospects of Nanoscience with Nanocrystals. *ACS Nano* **2015**, *9*,1012-1057.

(3) Reiss, P.; Carriere, M.; Lincheneau, C.; Vaure, L.; Tamang, S. Synthesis of Semiconductor Nanocrystals, Focusing on Nontoxic and Earth-Abundant Materials. *Chem. Rev.* **2016**, *116*, 10731-10819.

(4) Tamang, S.; Linchemeau, C.; Hermans, Y.; Jeong, S.; Reiss, P. Chemistry of InP Nanocrystal Syntheses. *Chem. Mater.* **2016**, *28*, 2491-2506.

(5) Xu, G.; Zeng, S.; Zhang,B.; Swihart, M. T.; Yong, K.; Prasad, P. N. New Generation Cadmium-Free Quantum Dots for Biophotonics and Nanomedicine. *Chem. Rev.* **2016**, *116*, 12234-12327.

(6) Micic, O. I.; Cheong, H. M.; Fu, H.; Zunger, A.; Sprague, J. R.; Mascarenhas, A.; Nozik, A. J. Size-Dependent Spectroscopy of InP Quantum Dots. *J. Phys. Chem. B* **1997**, *101*,4904-4912.

(7) Fu, H.; Zunger A. InP Quantum Dots: Electronic Structure, Surface Effects, and the Redshifted Emission. *Phys. Rev. B* **1997**, *56*, 1496-1508.

(8) Li, Y.; Hou, X.; Dai, X.; Yao, Z.; Lv, L.; Jin, Y.; Peng, X. Stoichiometry-Controlled InP-Based Quantum Dots: Synthesis, Photoluminescence, and Electroluminescence. *J. Am. Chem. Soc.* **2019**, *141*, 6448-6452.

(9) Crisp, R. W.; Kirkwood, N.; Grimaldi, G.; Kinge, S.; Siebbeles, L. D. A.; Houtepen A. J. Highly Photoconductive InP Quantum Dots Films and Solar Cells. *ACS Appl. Energy Mater.* **2018**, *1*, 6569-6576.

(10) Zhang, J.; Wang, J.; Yan, T.; Peng, Y.; Xu, D. J.; Deng, D. W. InP/ZnSe/ZnS Quantum Dots With Strong Dual Emissions: Visible Excitonic Emission and Near-Infrared Surface Defect Emission and Their Application in in Vitro and in Vivo Bioimaging. *J. Mater. Chem. B* **2017**, *5*, 8152-8160.

(11) Ikezawa, M.; Pal, B.; Masumoto, Y.; Ignatiev, I.V.; Verbin, S. Y.; Gerlovin, I. Y. Submillisecond Electron Spin Relaxation in InP Quantum Dots. *Phys. Rev. B* **2005**, *72*, 153302.

(12) Yang, X.; Zhao, D.; Leck, K. S.; Tan, S. T.; Tang, Y. X.; Zhao, J.; Demir, H. V.; Sun, X. W. Full Visible Range Covering InP/ZnS Nanocrystals with High Photometric Performance and Their Application to White Quantum Dot Light-Emitting Diodes. *Adv. Mater* **2012**, *24*, 4180-4185.

(13) Micic, O. I.; Ahrenkiel, S. P. ; Nozik, A. J. Synthesis of Extremely Small InP Quantum Dots and Electronic Coupling in Their Disordered Solid Films. *Appl. Phys. Lett.* **2001**, *78*, 4022-4024.

(14) Stein, J. L. ; Mader, E. A.; Cossairt, B. M. Luminescent InP Quantum Dots with Tunable Emission by Post-Synthetic Modification with Lewis Acids. *J. Phys. Chem. Lett.* **2016**, *7*, 1315-1320.

(15) Tessier, M. D.; De Nolf, K.; Dupont, D.; Sinnaeve, D.; De Roo, J.; Hens, Z. Aminophosphines: A Double Role in the Synthesis of Colloidal Indium Phosphide Quantum Dots. *J. Am. Chem. Soc.* **2016**, *138*, 5923-5929.

(16) Hettick, M.; Li, H.; Lien, D.-H.; Yeh, M.; Yang, T.-Y.; Amani, M.; Gupta, N.; Chrzan,

D.C.; Chueh, Y.-L.; Javey, A. Shape-Controlled Single-Crystal Growth of InP at Low Temperatures Down To 220 C. *Proc. Natl. Acad. Sci. USA* **2020**, *117*, 902-906.

(17) Biadala, L.; Siebers, B.; Beyazit, Y.; Tessier, M. D.; Dupont, D.; Hens, Z.; Yakovlev D. R.; Bayer, M. Band-Edge Exciton Fine Structure and Recombination Dynamics in InP/ZnS Colloidal Nanocrystals. *ACS Nano* **2016**, *10*, 3356-3364.

(18) Rabouw, F. T.; de Mello Donega, C. Excited-State Dynamics in Colloidal Semiconductor Nanocrystals. *Top. Curr. Chem. (Z)* **2016**, *374*, 58.

(19) Brodu, A.; Ballottin, M. V.; Buhot, J.; Harten, E. J.; Dupont, D.; Porta, A. L.; Prins, P. T.; Tessier, M. D.; Versteegh, M. A. M.; Zwiller, V.; *et al.* Exciton Fine Structure and Lattice Dynamics in InP/ZnSe Core/Shell Quantum Dots. *ACS Photonics* **2018**, *5*, 3353-3362.

(20) Kim, Y.; Ham, S.; Jang, H.; Min, J.H.; Chung, H.; Lee, J.; Kim, D.; Jang, E. Bright and Uniform Green Light Emitting InP/ZnSe/ZnS Quantum Dots for Wide Color Gamut Displays. *ACS Appl. Nano Mater.* **2019**, 2, 1496-1504.

(21) Won, Y.-H.; Cho, O.; Kim, T.; Chung, D.-Y.; Kim, T.; Chung, H.; Jang, H.; Lee, J.; Kim, D.; Jang, E. Highly Efficient and Stable InP/ZnSe/ZnS Quantum Dot Light-Emitting Diodes. *Nature* **2019**, *575*, 634-638.

(22) Janke, E. M.; Williams, N. E.; She, C.; Zherebetskyy, D.; Hudson, M. H.; Wang, L.; Gosztola, D. J.; Schaller, R. D.; Lee, B.; Sun, C.; *et al.* Origin of Broad Emission Spectra in InP Quantum Dots: Contributions from Structural and Electronic Disorder. *J. Am. Chem. Soc.* **2018**, *140*, 15791-15803.

(23) Thomas, A.; Sandeep, K.; Somasundaran, S. M.; Thomas, K. G. How Trap States Affect Charge Carrier Dynamics of CdSe and InP Quantum Dots: Visualization through Complexation with Viologen. *ACS Energy Lett.* **2018**, *3*, 2368-2375.

(24) Mićić, O. I.; Nozik, A. J.; Lifshitz, E.; Rajh, T.; Poluektov, O. G.; Thurnauer, M. C. Electron and Hole Adducts Formed in Illuminated InP Colloidal Quantum Dots Studied by Electron Paramagnetic Resonance. *J. Phys. Chem. B* **2002**, *106*, 4390-4395.

(25) Langof, L.; Ehrenfreund, E.; Lifshitz, E.; Micic, O. I.; Nozik, A. J. Continuous-Wave and Time-Resolved Optically Detected Magnetic Resonance Studies of Nonetched/Etched InP Nanocrystals. *J. Phys. Chem. B* **2002**, *106*, 1606-1612.

(26) Graf, P.A.; Kim, K.; Jones, W.B.; Wang, L.W. Surface Passivation Optimization Using DIRECT. *J. Comput. Phys.* **2007**, *224*, 824-835.

(27) Wang, L.-W.; Zunger, A. Local-Density-Derived Semiempirical Pseudopotentials. *Phys. Rev. B* **1995**, *51*, 17398-17416.

(28) Franceschetti, A.; Fu, H.; Wang, L. W.; Zunger, A. Many-Body Pseudopotential Theory of Excitons in InP and CdSe Quantum Dots. *Phys. Rev. B* **1999**, *60*, 1819-1829.

(29) Wang, L. W.; Califano, M.; Zunger, A.; Franceschetti, A. Pseudopotential Theory of Auger Processes in CdSe Quantum Dots. *Phys. Rev. Lett.* **2003**, *91*, 056404.

(30) Califano, M. Direct and Inverse Auger Processes in InAs Nanocrystals: Can the Decay Signature of a Trion Be Mistaken for Carrier Multiplication? *ACS Nano* **2009**, *3*, 2706-2714.

(31) Although this is not a realistic configuration, it represents a proof of concept to show the effect of surface P atoms.

(32) Yu, Z.; Li, J.; O'Connor, D. B.; Wang, L.-W.; Barbara, P. F. Large Resonant Stokes Shift in CdS Nanocrystals. *J. Phys. Chem. B* **2003**, *107*, 5670-5674.

(33) Ramsden, J. J.; Webber, S. E.; Grätzel M. Luminescence of Colloidal Cadmium Sulfide Particles in Acetonitrile and Acetonitrile/Water Mixtures. *J. Phys. Chem.* **1985**, *89*, 2740-2743.

(34) Hässelbarth, A.; Eychmüller, A.; Weller, H. Detection of Shallow Electron Traps in Quantum Sized CdS by Fluorescence Quenching Experiments. *Chem. Phys. Lett.* **1993**, *203*, 271-276.

(35) Sapra, S.; Mayilo, S.; Klar, T. A.; Rogach, A. L.; Feldmann, J. Bright White-Light Emission from Semiconductor Nanocrystals: by Chance and by Design. *Adv. Mater.* **2007**, *19*, 569-572.

(36) Hussein, M. T.; Kasim, T.; Abdulsattar, M. A.; Kaka, A. K. Density Functional Theory Study of InP Quantum Dot and Oxidized Surface. *IJAIEM* **2014**, *3*, 1-8.

(37) We define as "dark" any state whose optical matrix element connecting it to the $|0h;0e\rangle$ state is over 3 orders of magniture smaller than that relative to the absorption edge transition.

(38) Gong, K.; Zeng, Y.; Kelley, D. F. Extinction Coefficients, Oscillator Strengths, and Radiative Lifetimes of CdSe, CdTe, and CdTe/CdSe Nanocrystals. *J. Phys. Chem. C* **2013**, *117*, 20268-20279.

(39) Califano, M.; Rodosthenous, P. Theoretical Characterization of Gasb Colloidal Quantum Dots and Their Application to Photocatalytic CO_2 Reduction with Water. *ACS Appl. Mater. Interfaces* **2019**, *11*, 640-646.

(40) Micic, O. I.; Smith, B. B.; Nozik, A. J. Core-Shell Quantum Dots of Lattice-Matched ZnCdSe2 Shells on InP Cores: Experiment and Theory. *J. Phys. Chem. B* **2000**, *104*, 12149-12156.

(41) Rowland, C. E.; Liu, W.; Hannah, D. C.; Chan, M. K. Y.; Talapin, D. V.; Schaller, R. D. Thermal Stability of Colloidal InP Nanocrystals: Small Inorganic Ligands Boost High-Temperature Photoluminescence. *ACS Nano* **2014**, *8*, 977-985.

(42) Mnoyan, A. N.; Kirakosyan, A. Gh.; Kim, H.; Jang, H. S.; Jeon, D. Y. Electrostatic Stabilized InP Colloidal Quantum Dots with High Photoluminescence Efficiency. *Langmuir* **2015**, *31*, 7117-7121.

(43) Micic, O. I.; Sprague, J.; Lu, Z.; Nozik, A. J. Highly Efficient Band-Edge Emission from InP Quantum Dots. *Appl. Phys. Lett.* **1996**, *68*, 3150-3152.

(44) Li, H.; Jia, C.; Meng, X.; Li, H. Chemical Synthesis and Applications of Colloidal Metal Phosphide Nanocrystals. *Front. Chem.* **2019**, *6*, 652.

(45) Shen, W.; Tang, H.; Yang, X.; Cao, Z.; Cheng, T.; Wang, X.; Tan, Z.; You, J.; Deng, Z. Synthesis of Highly Fluorescent InP/ZnS Small-Core/Thick-Shell Tetrahedral-Shaped Quantum Dots for Blue Light-Emitting Diodes. *J. Mater. Chem. C* **2017**, *5*, 8243-8249.

(46) Sills, A.; Harrison, P.; Califano, M. Exciton Dynamics in InSb Colloidal Quantum Dots. *J. Phys. Chem. Lett.* **2016**, *7*, 31-35.

(47) Chang, A. Y.; Liu, W.; Talapin, D. V.; Schaller, R. D. Carrier Dynamics in Highly Quantum-Confined, Colloidal Indium Antimonide Nanocrystals. *ACS Nano* **2014**, *8*, 8513-8519.

(48) Klimov, V. I. Optical Nonlinearities and Ultrafast Carrier Dynamics in Semiconductor Nanocrystals. *J. Phys. Chem. B* **2000**, *104*, 6112-6123.

(49) Robel, I.; Gresback, R.; Kortshagen, U.; Schaller, R. D.; Klimov, V. I. Universal Size-Dependent Trend in Auger Recombination in Direct-Gap and Indirect-Gap Semiconductor Nanocrystals. *Phys. Rev. Lett.* **2009**, *102*, 177404.

(50) Li, Y.-H.; Walsh, A.; Chen, S.; Yin, W.-J.; Yang, J.-H.; Li, J.; Da Silva, J.L.F.; Gong, X.G.; Wei, S.-H. Revised *Ab Initio* Natural Band Offsets of All Group IV, II-VI, and III-V Semiconductors. *Appl. Phys. Lett.* **2009**, *94*, 212109.

(51) Adam, S.; Talapin, D.V.; Borchert, H.; Lobo, A.; McGinley, C.; de Castro, A.R.B.; Haase, M.; Weller, H.; Möller, T. The Effect of Nanocrystal Surface Structure on the Luminescence Properties: Photoemission Study of HF-etched InP Nanocrystals. *J. Chem. Phys.* **2005**, *123*, 084706.